# Topographic Disturbance in Viscous Shear Flow

By Takehiko Satomura

*Meteorological Research Institute, 1-1, Nagamine, Yatabe, Tsukuba, Ibaraki 305, Japan*
*(Manuscript received 21 February 1986, in revised form 17 August 1986)*

## Abstract

The initial-value problem corresponding to perturbed viscous shear flow in shallow water over topography is solved both analytically and numerically. A formal solution is obtained analytically by using the Fourier-Laplace transform. On the other hand, a numerical solution is obtained for Froude number $Fr$=0.1 and a basic flow $U$=tanh($y$) by time integration. Both spatial and temporal behavior of the solution are studied.

The stability of shear flows which are unstable in an inviscid fluid over a flat bottom changes with the strength of the friction; it varies from unstable to stable through a resonance between the topographic forcing and a barotropic wave. The structure of the disturbance is very similar to the unstable barotropic wave as long as the friction is slightly greater than the resonance point. It is supplied with energy from the basic shear flow through the Reynolds stress. Furthermore, a vortex remains in the basic shear zone when the topography moves across the flow. The structure of this vortex is also similar to the unstable barotropic wave and its energy is supplied from the shear flow. Thus, the vortex has a long life time against the friction.

If the friction is large, the disturbance directly reflects the topographic forcing. The structure is similar to gravity waves and the energy is supplied from the topographic forcing.

A comparison with the vortex observed in the atmosphere is also described.

## 1. Introduction

The purpose of this investigation is to examine effects of topography on a viscous shear flow and to present a possible mechanism of formation of mesoscale vortices.

In a number of papers dealing with stability of the flow, the characteristics of horizontal shear flows are investigated extensively. Especially, through series of theoretical papers (Blumen, 1970; Blumen *et al.* 1975; Drazin and Davey, 1977; Satomura, 1981a, b), the following turned out to be clear: 1) a necessary condition for instability is that Froude number $Fr$ (or Mach number $Ma$) $\geqq 1$ or $U/U'' \leqq 0$ in a region of the fluid; 2) if $Fr<1$ and $U/U''<0$, the growth rate is reduced by the divergence effect, still the flow is barotropically unstable; 3) if $Fr>1$, gravity waves (or acoustic waves) become unstable. They do not relate with the point of inflection but with strong divergence. Using a numerical model, Satomura (1982) inquired further into effects of nonlinearity and viscosity on the instability of a divergent shear flow for $Fr$=5. He found that gravity waves mixed the average momentum permanently.

Although the papers cited above showed effects of divergence on stability of flows, they do not discuss effects of external forcing on a horizontal shear flow. These effects were examined in another series of papers concerned with lee waves (Blumen and McGregor, 1976; Blumen and Dietze, 1981, 1982). In these papers, they found linear steady solutions in a horizontal shear flow in an inviscid fluid. They also showed that wave energy is primarily contained within a horizontal strip as a consequence of the cross-stream variation of the basic flow and that Eliassen-Palm flux depends on features of the mountain. But the steadiness of the system was assumed, whereas the basic flow $U$=sech($y$) is barotropically unstable. Thus, it would be interesting to investigate effects of

the forcing on a shear flow without the assumption $\partial/\partial t=0$, while they justified the assumption by frequent observations of steady lee waves (Blumen, 1986; private communication).

In conditions of mild weather, mesoscale vortices, the formation mechanism of which is another motivation of this paper, are observed in the planetary boundary layer of the atmosphere. Using wind towers, Wendell (1972) observed vortices over a fishhook-shaped valley in Idaho, USA. Those vortices appeared at night and they had diameters of about 50km. Harada (1981) also observed vortices over Kanto plains in Japan (hereafter, we call them "Harada's vortex"). He found that the horizontal and vertical scale of the vortex are about 100km and 1km, respectively. The vortex moved slowly from the west to the east over the plain. Recently, other vortices were also found in Hokkaido, Japan (Kimura, 1986), in Victoria, Australia (Abbs, 1986), and in Colorado, USA (Abbs and Pielke, 1986).

These studies also discussed formation mechanisms of the vortices. Both Wendell (1972) and Harada (1981) suggested by data analysis that the diurnal differential heating and the mechanical effect of local topography would cause the formation of the vortex. Using a realistic nonlinear numerical model, Abbs (1986) indicated enhanced convergence resulting from the interaction of two different sea breezes as the cause of the vortex formation, and Abbs and Pielke (1986) suggested heating effects coupled with convergence of the low-level flow. On the other hand, Kimura (1986) also used three-dimensional local wind model and concluded that the most important cause of Harada's vortex is stretching of vortex tubes in a shear zone, which is created in the front of a mountain wind, by a small valley or a "crater". While the mechanisms proposed by these studies are rather diverse, we notice an element common in them: vorticity concentration due to the convergence forced by some external causes such as a crater or the interaction of sea breezes. Thus, from the point of the formation mechanism of mesoscale vortices, it would be also useful to study basic effects of forcing on a shear flow by using a simple model.

In this paper, we will use the shallow water model because it is the simplest model suitable for our purpose; this model includes an effect of divergence, a horizontal shear flow, and a steady forcing by bottom topography. We will present the linearized equation of the model in section 2. In section 3, the analytical solution is derived by the Fourier-Laplace transform, and basic characteristics of the solution are examined. In section 4, the linear equations are numerically integrated in time. It will be shown that a large vortex similar to the barotropically unstable wave is formed over the forcing area. We will also discuss the structure and the energetics of the disturbance.

## 2. Basic Equations

Consider a disturbance in a plane parallel flow $U^*(y^*)$ over the small-amplitude topography described by $z^*=h_0^*(x^*, y^*)$ as shown in Fig. 1, where the basic flow $U^*$ is in the $x^*$ direction and varies in the transverse direction $y^*$. By introducing a velocity scale $U_0$ and a length scale L, both of which are straightforwardly derived from the basic flow, and taking a depth scale $D_0$ from the basic depth of the fluid, we can write the dimensionless coordinates, time, velocity, surface displacement, and bottom topography as

$$(x, y)=(x^*, y^*)/L, \quad t=t^*U_0/L,$$
$$U(y)=U^*(y^*)/U_0, \quad (u, v)=(u^*, v^*)/U_0,$$
$$h=h^*/D_0, \quad h_b=h_b^*/D_0. \tag{2.1}$$

The perturbation equations for the disturbance are written as

$$\frac{\partial u}{\partial t}+U\frac{\partial u}{\partial x}+v\frac{dU}{dy}+\frac{1}{F_r^2}\frac{\partial h}{\partial x}=\mathcal{F}_u,$$
$$\frac{\partial v}{\partial t}+U\frac{\partial v}{\partial x}+\frac{1}{F_r^2}\frac{\partial h}{\partial y}=\mathcal{F}_v, \tag{2.2}$$
$$\frac{\partial h}{\partial t}+U\frac{\partial h}{\partial x}+\frac{\partial u}{\partial x}+\frac{\partial v}{\partial y}=U\frac{\partial h_b}{\partial x}+\mathcal{F}_h,$$

where $Fr=U_0/\sqrt{gD_0}$ is the Froude number, $g$ is the gravity acceleration, $\mathcal{F}_u$ and $\mathcal{F}_v$ are friction terms, and $\mathcal{F}_h$ is a dissipation term for the surface displacement. The explicit forms of $\mathcal{F}_u$, $\mathcal{F}_v$, and $\mathcal{F}_h$ will be specified later. It is worth noting that the bottom topography is of the same order

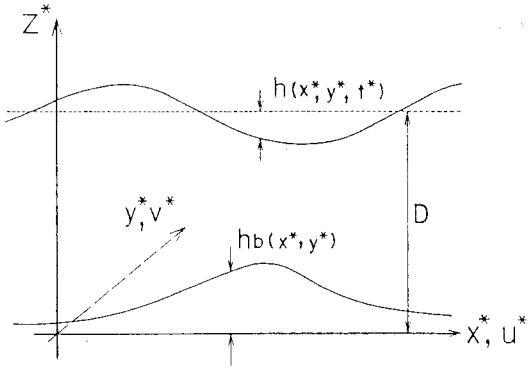


Fig. 1 Shallow water model.

as the perturbations. This is implicitly assumed in (2.2).

## 3. Analytical treatment

As long as $h_b$ is independent of time and

$$O(h_b)=O(u)=O(v),$$

we should not assume a form

$$q=q'(y)\exp[ik(x-ct)], \tag{3.1}$$

for each component $q$ of the perturbation quantities $(u, v, h)$ because it leads to the conclusion $c$=0. If the basic flow satisfies the sufficient condition of instability, unstable modes, if they exist, would grow exponentially with time and dominate the flow pattern. These unstable modes are neglected if we solve (2.2) under the condition $c$=0. It indicates that the a priori assumption $c$=0 loses the generality. Thus, instead of the normal mode analysis such as (3.1), we treat (2.2) as an initial-value problem.

In order to handle the problem more easily, we specify the damping terms in this section as

$$\begin{aligned}\mathcal{F}_u&=-\nu^R u,\\ \mathcal{F}_v&=-\nu^R v,\\ \mathcal{F}_h&=-\nu^R h.\end{aligned} \tag{3.2}$$

To solve the initial-value problem, take the Fourier transform with respect to $x$ and the Laplace transform with respect to $t$. Thus, let

$$q_{pk}(y)=\int_0^\infty\int_{-\infty}^\infty q(x,y,t)e^{-ikx}dx e^{-pt}dt. \tag{3.3}$$

Equation (2.2) becomes

$$(s+ikU)u_{pk}+v_{pk}\frac{dU}{dy}-u_{ik}+\frac{ik}{F_\tau^2}h_{pk}=0,$$

$$(s+ikU)v_{pk}-v_{ik}+\frac{1}{F_\tau^2}\frac{dh_{pk}}{dy}=0, \tag{3.4}$$

$$(s+ikU)h_{pk}-h_{ik}+iku_{pk}-\frac{dv_{pk}}{dy}=\frac{ik}{p}Uh_{bk},$$

where

$$q_{ik}=\int_{-\infty}^\infty q(x,y,0)e^{-ikx}dx,$$

$$h_{bk}=\int_{-\infty}^\infty h_b(x,y)e^{-ikx}dx,$$

$$s=p+\nu^R.$$

For simplicity, let $u_{ik}=v_{ik}=0$. By eliminating $u_{pk}$ and $v_{pk}$, eq. (3.4) is reduced to

$$\frac{d}{dy}\left\{\frac{1}{(s+ikU)^2}\frac{dh_{pk}}{dy}\right\}-\left\{F_\tau^2+\frac{k^2}{(s+ikU)^2}\right\}h_{pk}=\frac{F_\tau^2}{s+ikU}\left(h_{ik}-\frac{ikU}{p}h_{bk}\right). \tag{3.5}$$

The boundary condition is

$$h_{pk}(\pm a)=0. \tag{3.6}$$

Further, to keep things simple, we take

$$h_{bk}=\hat{h}_{bk}\delta(y-y_b)$$

where $\delta(y)$ is the Dirac delta function and $\hat{h}_{bk}$ depends only upon $k$. Then, the solution of (3.5) under the condition (3.6) is written as

$$\begin{aligned}h_{pk}(y)&=-F_\tau^2\int_{-a}^{a}\frac{h_{ik}(y_G)}{s+ikU(y_G)}G(y,y_G)dy_G\\&\quad+\frac{ikF_\tau^2}{p}\frac{\hat{h}_{bk}U(y_b)}{s+ikU(y_b)}G(y,y_b),\end{aligned} \tag{3.8}$$

where $G(y, y_b)$ is Green's function of (3.5) with the condition (3.6) (see Appendix A for derivation). The Laplace inversion theorem gives

$$\begin{aligned}h_k(y,t)&=\frac{1}{2\pi i}\int_{C_L}h_{pk}(y)e^{pt}dp\\&=-\frac{F_\tau^2}{2\pi i}\int_{C_L}\int_{-a}^{a}\frac{h_{ik}(y_G)}{s+ikU(y_G)}G(y,y_G)e^{pt}dy_G dp\\&\quad+\frac{kF_\tau^2}{2\pi}\int_{C_L}\frac{\hat{h}_{bk}U(y_b)}{p(s+ikU(y_b))}G(y,y_G)e^{pt}dp,\end{aligned} \tag{3.9}$$

with $C_L$ parallel to the imaginary axis and to the right of all singularities of the integrand.

In order to determine time behavior of $h_k$, we must know the characteristics of the singularities.

There are three types of singularities (see Appendix A):

(i) $p+\nu^R+ikU=0$, pole plus branch point,
(ii) $\mathcal{D}(p+\nu^R, k)=0$, pole,
(iii) $p=0$, pole. (3.10)

At first, let us see the characteristics in the inviscid situation. The singularities of the type (i) give the continuum modes which do not grow in an inviscid fluid as discussed originally by Case (1960), who also used the Fourier-Laplace transform to solve an initial-value problem.

Because the equation $\mathcal{D}=0$ is the eigenvalue-equation of the barotropic instability, the singularities of the type (ii) give rise to the exponential behavior which would be expected of discrete normal modes in an inviscid fluid as discussed also by Case (1960). These eigenvalues of type (ii) are divided into two eigen-modes: barotropic modes and gravity modes. The gravity modes have non-zero phase velocity and are neutral as long as $Fr<1$ (Satomura, 1981a). The barotropic modes, on the other hand, grow as an exponent of time (*i.e.* $p$ is real and corresponds to the growth rate) for $Fr<1$ in an inviscid fluid because the first term on the right hand side of (3.9) is not affected by the topography(#1). Thus we discuss barotropic modes only for the type (ii) modes.

The singularity of the type (iii) arises from the bottom topography $h_b$ and it gives a steady topographic mode.

Next, let us see the characteristics in the viscous case. In general, the Rayleigh damping of (3.2) decreases growth rates. Since the continuum modes (type (i)) would damp exponentially with time, we shall discuss only the modes of types (ii) (*i.e.* barotropic modes) and (iii) (topographic modes) below.

As $\nu^R$ increases the growth rate $p$ of the barotropic mode decreases and equals zero at $\nu^R=\nu_k^R=r_k$ where $r_k$ is the largest growth rate at wavenumber $k$ in an inviscid fluid. In this case, the singularity of type (ii) for $\nu^R=\nu_k^R$ coincides with that of type (iii), and the order of the pole $p=0$ becomes two(#2). This gives a disturbance which grows proportionally with $t$, according to the Laplace inverse transform. This is a resonance between the barotropic unstable mode and the topography.

In the case $\nu^R>\nu_k^R$, we return to (3.9) and deform the contour of the inverse transform to the left. Then, (3.9) can be written by using (A.7) as

$$h_k(y,t) = \frac{kF_r^2}{2\pi}\int_{-i\infty-\nu^R+\varepsilon}^{i\infty-\nu^R+\varepsilon} h_{pk}(y)e^{pt}dp + \sum(\text{discrete exponential}) + \frac{ikF_r^2U(y_b)\hat{h}_{bk}[\phi_1(y>y_b)\phi_2(y<y_b)]}{(\nu^R+ikU(y_b))\mathcal{D}(\nu^R,k)}, \quad (3.11)$$

where $\epsilon$ is a small number. The second and third terms of the left-hand side arise from the poles of types (ii) and (iii), respectively. The first and second terms of the left-hand side of (3.11) damp with time, so that (3.11) becomes

$$h_k(y,t) = \frac{ikF_r^2U(y_b)\hat{h}_{bk}[\phi_1(y>y_b)\phi_2(y<y_b)]}{(\nu^R+ikU(y_b))\mathcal{D}(\nu^R,k)} \quad (3.12)$$

for $t\gg1$. Equation (3.12) indicates that the topographic mode only dominates the perturbation field if $\nu^R>\nu_k^R$. In the following, we will discuss the solution only in the case $\nu^R>\nu_k^R$, because the well-known barotropic waves grow and dominate the flow if $\nu^R<\nu_k^R$. Further, the numerical study on Harada's vortex performed by Kimura (1986) showed that small perturbations superposed on a shear flow in a mountain-wind front slowly decrease their amplitudes; this probably indicates $\nu^R>\nu_k^R$ in the case of Harada's vortex at least.

To find characteristics of the structure in the $y$ direction, consider two extremes,

(#1) It is interesting that unstable barotropic modes are not affected by small topography at all. But we do not discuss if further in this paper.

(#2) In shear flows such as $U=\tanh(y)$ or $U=\mathrm{sech}(y)$, the order of any zeros of $\mathcal{D}(p+\nu^R,k)$ would be expected to be one.

(a) $1 \gg \nu^R - \nu_k^R > 0$,

(b) $\nu^R \gg \nu_k^R$. (3.13)

In the case (a), $\mathcal{D}(\nu^R, k)$ would be

$$\mathcal{D}(\nu^R, k) \approx \mathcal{D}(\nu_k^R, k) = 0. \quad (3.14)$$

This indicates that $p$=0 nearly satisfies the eigenvalue-equation of the barotropic instability $\mathcal{D}$=0. Thus, the structure in the $y$ direction is similar not to the topographic forcing but to the unstable barotropic mode of the wavenumber $k$, although the mode itself is a steady mode forced by the topography.

On the other hand, in case (b), $\mathcal{D}(\nu^R, k)$ would be far from zero. Ths structure in the $y$ direction would not be similar to the unstable barotropic mode.

Next, in order to examine the structure in the $x$ direction, we apply the Fourier inverse transform to (3.12);

$$h(x, y, t) = \frac{1}{2\pi}\int_{-\infty}^{\infty} h_k(y, t) e^{ikx} dk$$

$$= \frac{1}{2\pi}\int_{-\infty}^{\infty} \frac{ikF_\gamma^2 U \hat{h}_{bk}[\phi_1(y > y_b)\phi_2(y < y_b)] e^{ikx} dk}{(\nu^R - ikU)\mathcal{D}(\nu^R, k)} \quad (3.15)$$

for $t \gg 1$.

Because $r_k$ reaches its maximum $r_{\max}$ at $k = k_c$, which is the maximum growth rate of the inviscid barotropic instability, we should consider the following extremes instead of (3.13):

(a′) $1 \gg \nu^R - \nu_c^R > 0$,

(b′) $\nu^R \gg \nu_c^R$, (3.16)

where $\nu_c^R = r_{\max}$.

First, we examine the case (a′). Because $\nu^R \approx \nu_c^R$, the integrand of (3.15) will have a pole at $k = k_a$ which is located near $k_c$ in the complex $k$ plane. Thus, (3.15) is evaluated approximately as

$$h(x, y, t) \approx \frac{ikaF_\gamma^2 U \hat{h}_{bk_a}[\phi_1\phi_2] e^{ik_a x}}{\nu^R - ik_a U} \cdot \left\{\lim_{k \to k_a} \frac{k - k_a}{\mathcal{D}(\nu^R, k)}\right\}, \quad (3.17)$$

where

$$\mathrm{Im}(k_a) \geqq 0 \quad \text{for } x \geqq 0,$$
$$< 0 \quad \text{for } x < 0. \quad (3.18)$$

The contribution to the integral of (3.15) from other zeros of $\mathcal{D}$ is expected to be small for $|x| \gg 1$ because the imaginary part of the poles will be larger than that of $k_a$. The contribution from the zero of $\nu^R + ikU$ is not considered, but it is probably small according to the results of the numerical simulation described in the next section.

It is indicated from (3.17) that the structure in the $x$ direction is periodic with wavenumber of $Re(k_a) \approx k_c$ and amplitude which decreases as $\exp[-|Im(k_a)|x]$. Again we find a similar structure to the most unstable barotropic mode, although this disturbance is the steady mode forced by the topography. This is an interesting result because the eigen-mode of the system finally dominates without any dependence on the forcing distribution.

In case (b′), the structure in the $x$ direction would strongly reflect the structure of the forcing as long as it does not vary significantly in the forced wavenumber range. This is confirmed by the numerical simulation.

## 4. Numerical treatment

To verify the theoretical discussion of the preceding section, we integrate eq. (2.2) numerically for $Fr$=0.1(#3).

We use a space-staggered and time-centered grid and the grid resolutions in the $x$ and $y$ directions are $\Delta x$=0.47 and $\Delta y$=0.4, respectively. The domain of integration is $-15 < x < 15$, $-10 < y < 10$, and boundary conditions in the $x$ and $y$ directions are cyclic and rigid walls, respectively. The length of the domain in the $x$ direction is about twice as long as the wavelength of the most unstable barotropic mode in an inviscid fluid.

We consider a basic flow

(#3) As mentioned in introduction, if $Fr$<1, growing modes are unstable barotropic modes only (Satomura, 1981a, b). Thus, we are able to fix the Froude number to a number less than unity without loss of generality.

$$U(y)=\tanh(y), \tag{4.1}$$

and the bell-shaped dent with circular contours

$$h_b(x,y)=\frac{-1}{(R^2/a^2-1)^{3/2}}, \tag{4.2}$$

where $R=\sqrt{x^2+(y+y_0)^2}$. In this model, we can specify the center of the dent, $(0,y_0)$, to any point in the $y$ axis. The parameter $a$ defines the scale of the forcing. In order to separate the forcing scale from the resonant or near resonant modes which have wavelengths of the order of 10, we set $a=0.5$.

In this section, we specify the damping term as

$$\mathcal{F}_u=\nu\nabla^2 u,$$
$$\mathcal{F}_v=\nu\nabla^2 v, \tag{4.3}$$
$$\mathcal{F}_h=0,$$

where

$$\nabla^2\equiv\frac{\partial^2}{\partial x^2}+\frac{\partial^2}{\partial y^2}.$$

The formulation (4.3) is more realistic than (3.1). The resonance phenomenon, however, will change because of the different dependence on wavenumber. In the present situation, it is difficult to determine the critical viscosity $\nu_c$ precisely. Instead of using the definition $\nu_c=r_{\max}$, we define $\nu_c$ such that, if $\nu>\nu_c$, the amplitude of every disturbance decreases to zero in the domain of integration. Then, it is possible to estimate $\nu_c$ by trial and error, and we find $0.25<\nu_c<0.3$. In the following discussion, the cases (a′) and (b′) are represented by $\nu=0.3$, $\nu=1.0$, respectively.

Three numerical experiments are performed. In exp. 1, we specify $y_0=0$ in (4.2) and $\nu=0.3$. This experiment will reveal the characteristics of the near-resonant mode. In exp. 2, we also specify $\nu=1.0$. This experiment will show the non-resonant mode. Finally, in exp. 3, we again set $\nu=0.3$ but

$$y_0=-5+0.3t,$$

which describes the relative movement of the dent to the basic flow. This experiment tests whether the near-resonant mode remains in the shear zone when the forcing moves away. This is regarded as a simplified model which roughly simulates the passage of the front of the mountain wind over a dent. While this experiment is oversimplified to simulate the "Harada's vortex", we expect it to give some ideas about the formation mechanism of the vortex.

EXP. 1: *Shear flow with viscosity slightly larger than the resonance*

Fig. 2(a) displays the structure of the perturbation velocity at $t=30$. While the flow converges at the upper-right and the lower-left sides of the dent, the flow pattern is very similar to the unstable nearly nondivergent disturbance shown in Fig. 3(a) and (b) for an inviscid fluid with a flat bottom; this disturbance is an unstable barotropic wave in essence. The scale of the perturbation is much larger than the topography and this is one of the characteristics of the near resonant mode. Further, we notice that the perturbation decreases in its strength gradually away from the dent. It confirms the approximate formula (3.18) qualitatively. The dominant wavenumber of this pattern, however, appears to be one half of $k_c$. This is due partly to higher-order differentiation in the damping term (4.3) and partly to finiteness of the domain. We discuss it briefly in Appendix B. As a whole, the structure and the largeness of the scale mentioned above agree with the analytical treatment discussed in the previous section.

Fig. 2(b) shows the disturbed flow $(U+u,v)$ at $t=30$, where $U=-U_m\tanh(y)$, and $U_m$ is twice as large as the maximum value of $u$ and $v$ in the whole domain. We see a vortex clearly around the dent. The horizontal scale of the composite vortex is much larger than the dent. We should note, however, $U_m$ is rather small compared with a limit of linearization and, hence the vortex would be emphasized in this figure.

At later time $t=50$, when the perturbation becomes almost steady, the flow pattern similar to the unstable barotropic wave becomes more dominant (Fig.4(a)) and the scale of the composite vortex appears to expand slightly (Fig. 4(b)).

It would be interesting to examine the energetics of this flow. By a short and straightforward calculation of (2.2), the energy equations are written as

$$\frac{dK_E}{dt}=[K_Z,K_E]-[K_E,P_E]-[K_E,\nu], \tag{4.4}$$

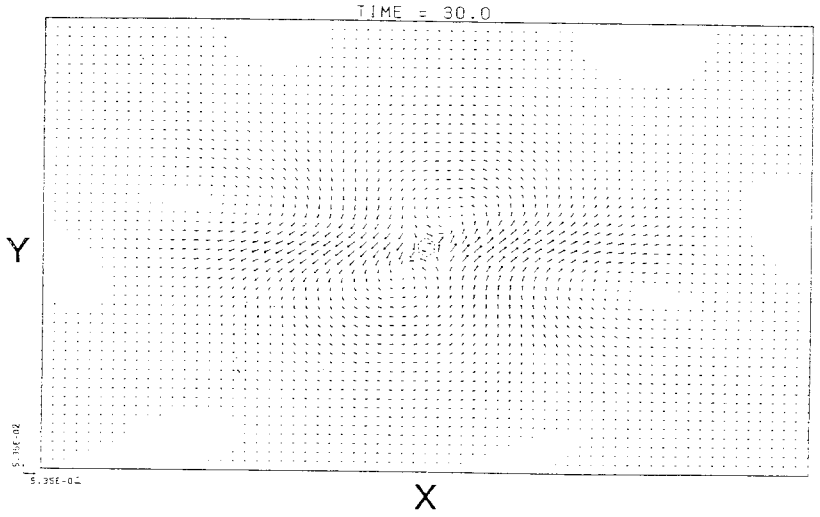


Fig. 2(a) Velocity of disturbance, $(u,v)$, at $t$=30 of exp. 1. Dotted circle at the center indicates a contour of the topography $h_b$=0.5.

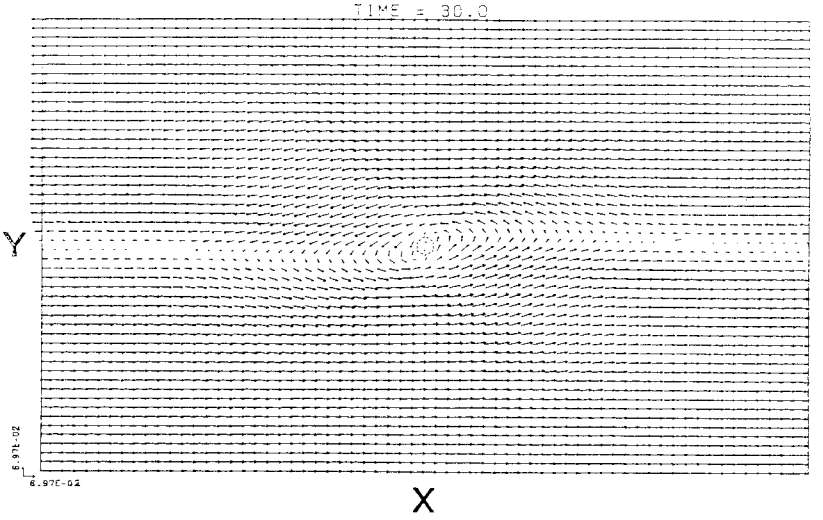


Fig. 2(b) Disturbed velocity, $(U+u,v)$, at $t$=30 of exp. 1. Dotted circle at the center indicates a contour of the topography $h_b$=0.5.

$$\frac{dP_E}{dt}=[K_E, P_E]+[h_b, P_E],$$

where

$$K_E\equiv\frac{1}{2}\int(u^2+v^2)dS$$

and

$$P_E\equiv\frac{1}{2F_r^2}\int h^2 dS$$

are the perturbation kinetic energy and the perturbation potential energy, respectively. The terms

$$[K_Z, K_E]\equiv-\int uv\frac{dU}{dy}dS$$

and

$$[K_E, P_E]\equiv-\frac{1}{F_r^2}\int h\left(\frac{\partial u}{\partial x}+\frac{\partial v}{\partial y}\right)dS$$

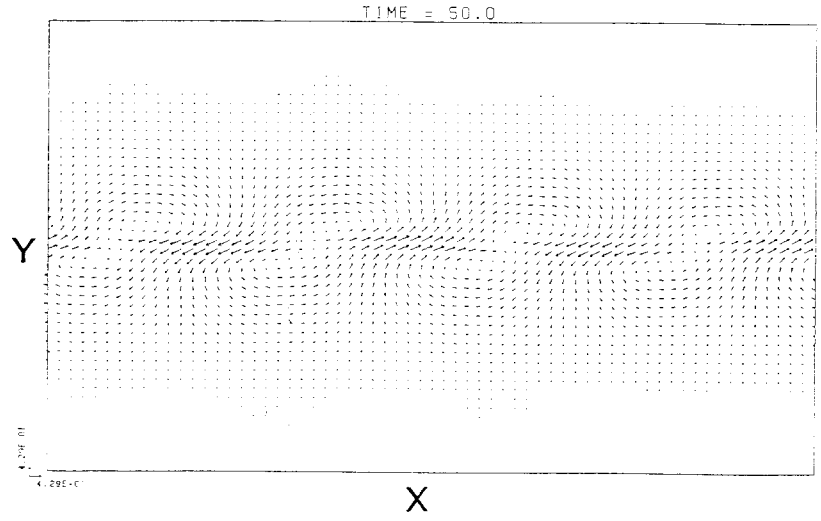


Fig. 3(a) Velocity of disturbance, $(u,v)$, of the barotropic instability for $Fr$= 0.1.

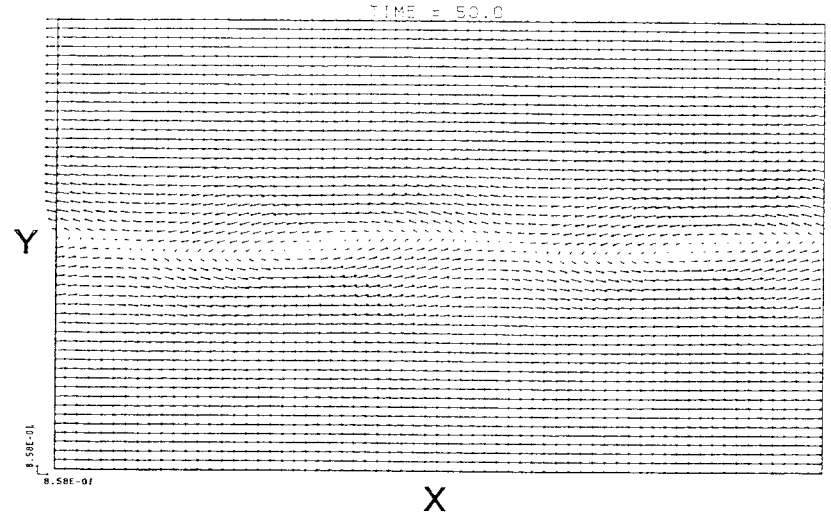


Fig. 3(b) Disturbed velocity, $(U+u,v)$, of the barotropic instability for $Fr$= 0.1.

represent the energy conversions from the mean kinetic energy $K_Z$ to $K_E$, and $K_E$ to $P_E$, respectively. The terms

$$[K_E,\nu]\equiv-\nu\int(u\nabla^2u-v\nabla^2v)dS$$

and

$$[h_b,P_E]\equiv\frac{1}{F_r^2}\int Uh\frac{\partial h_b}{\partial x}dS$$

represent the dissipation of $K_E$ by viscosity and the generation of $P_E$ by the topographic lifting, respectively.

The mean kinetic energy can be divided into two parts as Satomura (1981a) discussed. As far as the case we considered in this paper, however, the rate of the inner conversion of the two parts is found small and thus we do not discuss the inner conversion.

Fig. 5 shows the energy diagram at $t$=50.

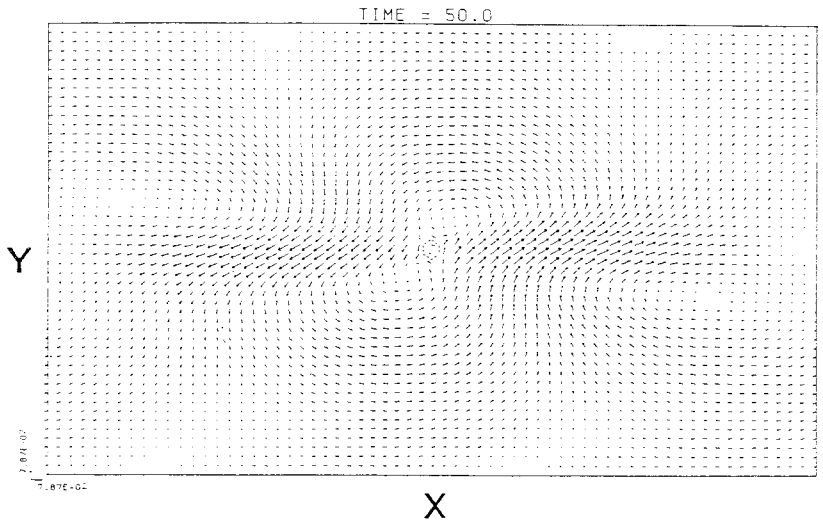


Fig. 4(a) Same as Fig. 2(a) but $t$=50.

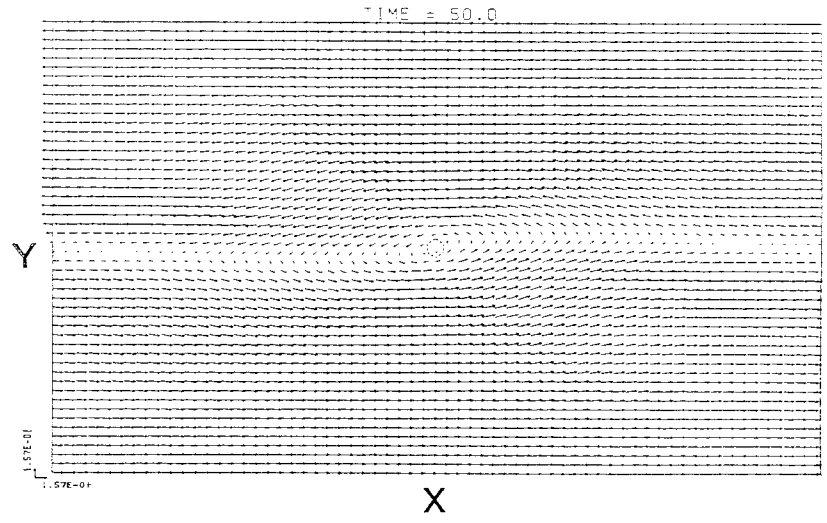


Fig. 4(b) Same as Fig. 2(b) but $t$=50.

It is evident that the perturbation is supplied with energy mainly not from the topographic forcing but from the mean kinetic energy. This fact is evidence that this mode is closely connected with barotropic instability and this is one of the characteristics of the near-resonant mode discussed in the preceding section.

The vorticity and the divergence of the perturbation field are shown in Fig. 6. We see that the divergence exceeds the vorticity near the dent but the vorticity comes to be dominant away from the dent. Thus, as a gross feature, the disturbed flow seems to be a barotropic vortex.

EXP. 2: *Shear flow with large viscosity*

Next, we show the velocity at $t$=50 in Fig. 7. It is clearly found that the scale of the perturbation is much smaller than that of exp. 1. We also find that the divergence and the convergence of the perturbation velocity is dominant. In fact, the maximum of the divergence is found to be more than ten times the maximum of the vorticity. The absolute values of the velocity,

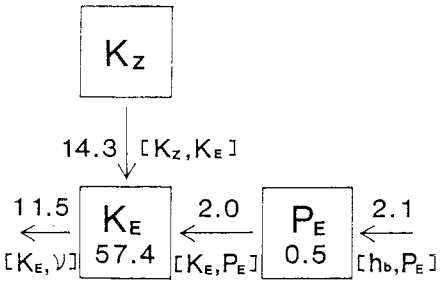


Fig. 5 Energy diagram of disturbance at $t$=50 for exp. 1.

divergence, and vorticity are, however, smaller than those of exp. 1.

The energy diagram is presented in Fig. 8. This diagram indicates that the energy conversion due to the Reynolds stress turns out to be negligibly small compared with the dissipation of kinetic energy. Alternatively, the potential energy supplied from the topographic forcing maintains the perturbation kinetic energy through the correlation between the divergence and the surface elevation. These characteristics are what we expect of a non-resonant mode from the discussion in the preceding section.

EXP. 3: *Shear flow over moving topography*

The velocity of the perturbation is illustrated in Fig. 9 at $t$=50. At this time, the dent has passed the shear zone and reaches the boundary at $y=10^{(\#4)}$. Thus, in almost all the domain, the topographic forcing is so small that it has scarcely any influence on the flow. We find, however, that a vortex is formed in the shear zone and that it has a similar structure to the unstable barotropic wave. This vortex began growing when the dent approached the shear zone and it turns out to be evident after the dent left the shear zone. In order to explore why the vortex is not diminished by the viscosity, let us turn to the energy diagram presented in Fig. 10. This diagram shows that the energy conversion $[K_E, P_E]$ is less than half of $[K_Z, K_E]$. Because the dent is far from the vortex, it can supply only little energy to the vortex. Thus, the vortex probably receives almost all the kinetic energy through the energy conversion $[K_Z, K_E]$. In other words, once the vortex is formed by the dent, it extracts the kinetic

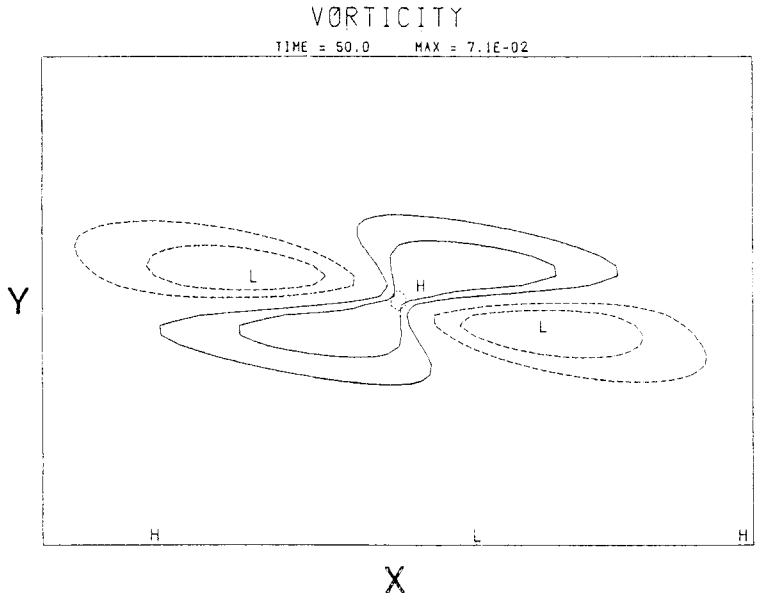


Fig. 6(a) Vorticity of disturbance at $t$=50 for exp. 1. Contour interval is 0.02.

(#4) The same calculation was performed in a larger domain, $(-15<x<15, -20<y<20)$, but the results changes little.

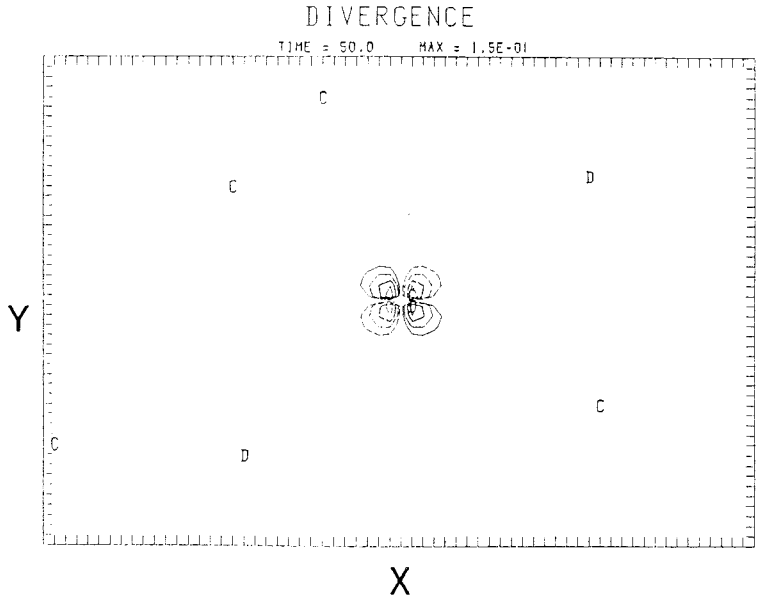


Fig. 6(b) Divergence of disturbance at $t$=50 for exp. 1. Contours are 0.02, 0.04, 0.08, 0.12.

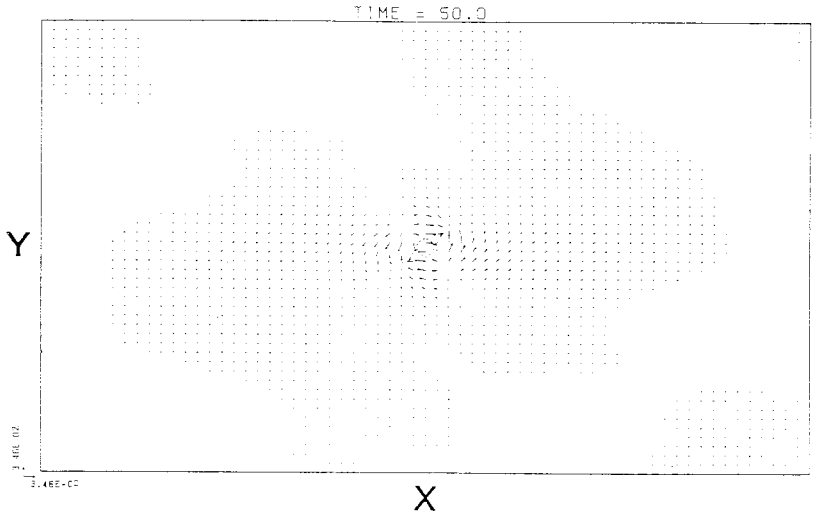


Fig. 7(a) Same as Fig. 4(a) but for exp. 2.

energy from the basic flow and can hold its strength against the viscous dissipation.

## 5. Summary and discussion

Through the use of the linearized shallow water equations, we have studied the response of plane parallel flow to steady forcing. Both analytical and numerical studies were performed for $Fr<1$.

The characteristics of the disturbance are summarized:

(a) If the basic flow is unstable over a flat bottom, the same flow over small topography is also unstable. The same disturbance as that over a flat bottom (*i.e.* eigen-

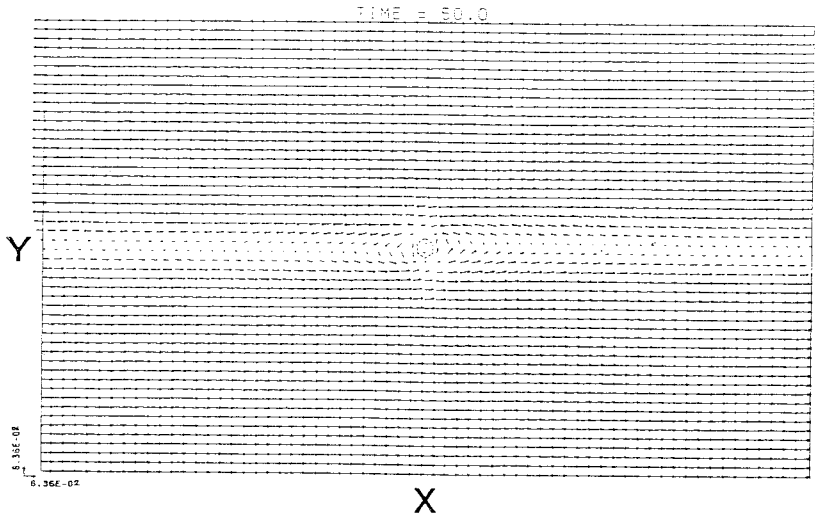


Fig. 7(b) Same as Fig. 4(b) but for exp. 2.

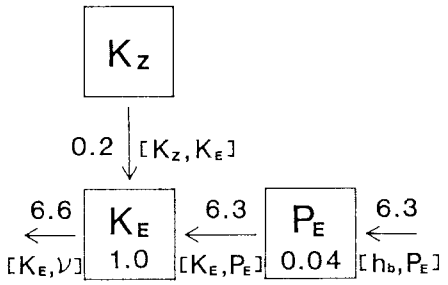


Fig. 8 Energy diagram of disturbance at $t$=50 for exp. 2.

mode) grows exponentially with time and finally dominates the steady topographic wave.

(b) If the friction equals the growth rate of the unstable mode in the inviscid flow, the eigen-mode will resonate with the topographic forcing. It grows as a power of $t$.

(c) If the friction is slightly greater than the growth rate, the flow is dominated by the steady topographic disturbance whose structure is similar to that of the unstable barotropic wave. The wavelength of the disturbance is much longer than the scale of the forcing, and it depends on the type of the damping. This disturbance is supplied with energy mainly through the energy conversion due to the Reynolds stress.

(d) When the dent goes across the shear zone, the vortex remains in the shear zone. It has a structure similar to that of the unstable barotropic wave and also receives its energy from the basic flow through the Reynolds stress. This fact interprets the long life of the vortex in the viscous fluid.

(e) If friction is much greater than the growth rate, the structure of the disturbance reflects topographic forcing. The disturbance receives its energy mainly from the forcing.

Encouraged by the result that the vortex much larger than the forcing is created in viscous shear flow, we will compare our disturbance with Harada's vortex in two aspects: the spatial and time scale of the disturbance. Of course, the energetics represents one of the important characteristics of the disturbance in this paper. But we cannot compare it with the observations or the numerical simulation because no calculation of energetics has been done yet.

Now, let us compare the orders of the spatial scales first. As discussed in the Appendix B, the longest wave in the region should appear if viscosity of the type $\nu\nabla^2 u$ acts on the waves. In the real atmosphere or the ocean, a basic current which satisfies the condition that it flows two-dimensionally over the topography in question and has appropriate shear probably exists only in a small region. This would provide

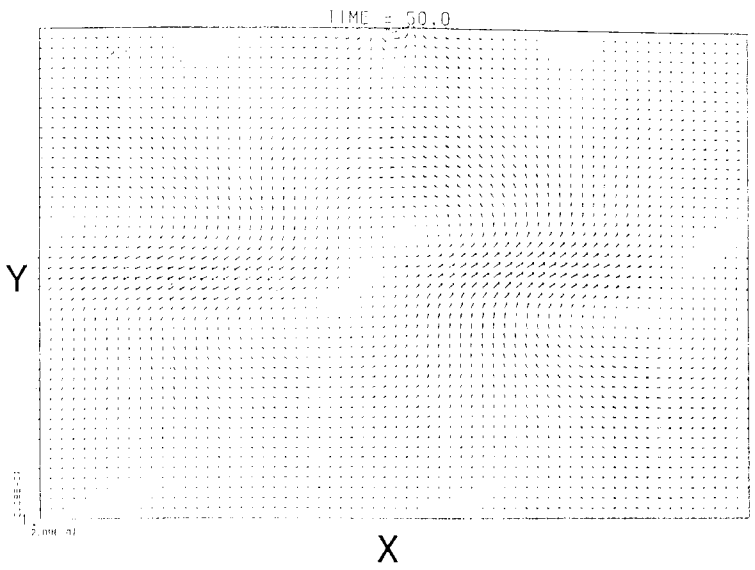


Fig. 9 Same as Fig. 4(a) but for exp. 3. The dent is going through the boundary at $y$=10 (the upper limit of the figure).

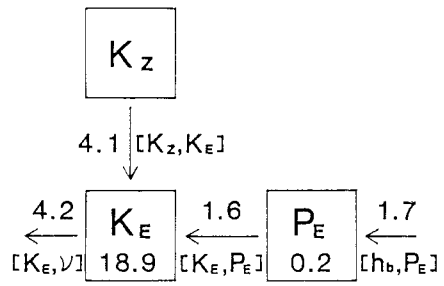


Fig. 10 Energy diagram of disturbance at $t$=50 for exp. 3.

the scale of the wave. In the case of Harada's vortex, the wind from the mountains located in the west of the plain has a large horizontal scale $\sim 10^2$ km. It does not contradict the discussion in this paper.

Next, let us compare the orders of the time scales. Numerical integration of this paper showed that the time scale of the growth of the disturbance is O(10) in a non-dimensional unit (2.1). On the other hand, since the wind from the mountains has a horizontal shear of the order of $3\times10^{-4}$sec$^{-1}$ (see, for example, Fig. 13 of Kimura, 1986), the time scale of $2\times10^4$ sec of Harada's vortex also corresponds to O(10) in non-dimensional unit. Thus, both time scales agree with each other.

In concluding the paper, the author wishes to point out the following as a generalization of the analytical results: Even when the basic flow is stable owing to the viscosity or the shear itself, disturbances similar to the eigen-modes of spatial scales different from the forcing would be observed if the forcing has the same phase velocity as that of the eigen-modes. This would be a reasonable generalization because the discussion in section 3 can be generalized to include many kinds of forcing. Some studies on baroclinic instability over topography (Pedlosky, 1981; Szoeke, 1983; Yoden and Mukougawa, 1983) support this generalization, although they are concerned with the interaction of neutral waves with topography in an inviscid fluid and we are concerned with a viscous fluid essentially. Further we suppose that the similar disturbance will appear even if the forcing has a slightly different velocity from that of the eigen-mode, since $\mathcal{D}(s,k)$ would be also small in this case. The results of Wakata and Uryu (1984), who calculated linear responses of a steady baroclinic wave over sinusoidal topography with Ekman layers, support this surmise.

**Acknowledgements**

The author is grateful to Dr. Kimura for leading the author into the problem of the topographic vortex and for helpful discussions. He would like to thank Dr. McGregor in CSIRO, Australia, and Dr. Niino in MRI for careful reading of the manuscript and their useful comments. The author also appreciate the reviewers' comments which helped to improve the revised version of this paper.

The computations were performed with the use of the HITAC-M200H computer of MRI.

## Appendix A

### Green's function

Let $\phi_i(y;k,s)$ $(i=1,2)$ be two linearly independent solutions of

$$\frac{d}{dy}\left\{\frac{1}{(s-ikU)^2}\frac{dh_{pk}}{dy}\right\}-\left\{F_r^2+\frac{k^2}{(s+ikU)^2}\right\}h_{pk}=0, \quad \text{(A-1)}$$

which is the homogeneous part of eq. (3.5) and coincides with eq. (2.6) of Satomura (1981a) by putting $s=-ikc$. The general solution can be expressed by

$$\phi=A\phi_1(y;k,s)+B\phi_2(y;k,s), \quad \text{(A-2)}$$

where A and B are constants. The explicit forms of $\phi_i$ around a singular point at $y=y_c$ where $s+ikU(y_c)=0$ have been given by Satomura (1981a) as

$$\phi_1=(y-y_c)^2\sum_{n=0}^{\infty}a_n(y-y_c)^n,$$
$$\phi_2=\gamma\phi_1\log(y-y_c)+\sum_{n=0}^{\infty}b_n(y-y_c)^n, \quad \text{(A-3)}$$

where $a_n$ and $b_n$ are expansion coefficients depending on $k$ and the profile of $U$, and $\gamma$ is a constant.

For there to be a non-trivial solution subject to the boundary condition (3.6) we must have

$$\mathcal{D}(k,s)\equiv\phi_1(-a;k,s)\phi_2(a;k,s)-\phi_2(-a;k,s)\phi_1(a;k,s)=0. \quad \text{(A-4)}$$

This serves to determine the discrete eigenvalues.

Next, define functions $\psi_1$ and $\psi_2$ as

$$\psi_1(y;k,s)\equiv\phi_1(y;k,s)\phi_2(a;k,s)-\phi_2(y;k,s)\phi_1(a;k,s),$$
$$\psi_2(y;k,s)\equiv\phi_1(y;k,s)\phi_2(-a;k,s)-\phi_2(y;k,s)\phi_1(-a;k,s). \quad \text{(A-5)}$$

Then, $\psi_1$ and $\psi_2$ satisfy eq. (A.1) and the conditions

$$\psi_1(a;k,s)=\psi_2(-a;k,s)=0. \quad \text{(A-6)}$$

Now we can construct Green's function $G(y,y_G)$ from $\psi_1,\psi_2$, and $\mathcal{D}$:

$$G(y,y_G)=\frac{[\psi_1(y>y_G)\psi_2(y<y_G)]}{\mathcal{D}(k,s)}, \quad \text{(A-7)}$$

where

$$[\psi_1(y>y_G)\psi_2(y<y_G)]=\begin{cases}\psi_1(y)\psi_2(y_G) & \text{for } y>y_G,\\ \psi_1(y_G)\psi_2(y) & \text{for } y<y_G.\end{cases} \quad \text{(A-8)}$$

## Appendix B

### Dominant scale and viscosity

Although the numerical results in exp. 1 and 2 are generally consistent with the analytical results, the wavelengths of the dominant modes are somewhat different from the analytical estimation. The reason for this difference is that we used the Rayleigh damping (3.2) in the analytical examination and the viscosity of the Laplacian type (4.3) in the numerical integration. As discussed in section 3, the resonant wavenumber for the Rayleigh friction is the same as that of the most unstable wave in an inviscid fluid, for the strength of the friction does not depend on the wavenumber (see Fig. B1). On the other hand, the effect of (4.3) varies with the wavenumber. We may estimate the viscous term as

$$\nu\nabla^2 q\approx-\nu\alpha k^2 q, \quad \text{(B-1)}$$

where $\alpha$ is a parameter that includes an effect of the wavenumber $l$ in the $y$ direction. If perturbations are sinusoidal also in the $y$ direction, $\alpha$ becomes

$$\alpha=1+\frac{l^2}{k^2} \quad \text{(B-2)}$$

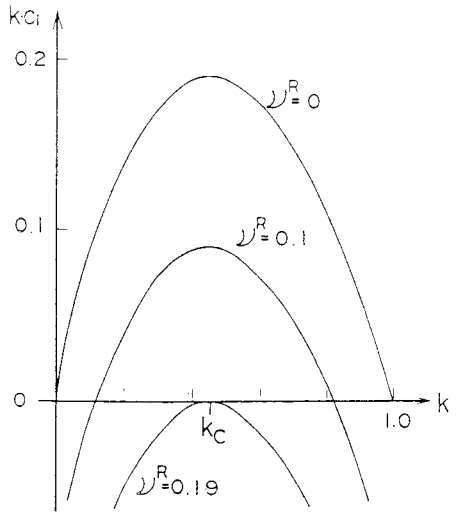


Fig. B1 Growth rates of barotropic instability with Rayleigh damping.

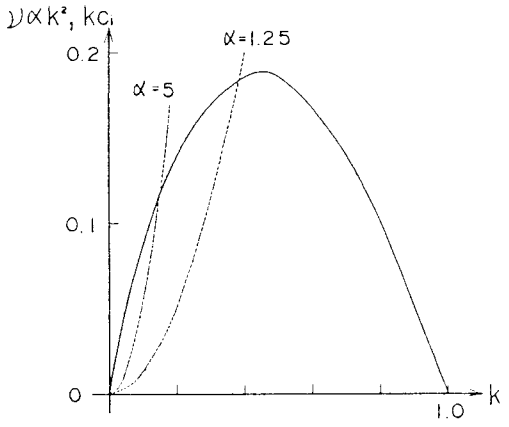


Fig. B2 Growth rates of barotropic instability and damping rates of viscosity $\nu\alpha k^2$ for $\alpha$=1.25 and 5.

Fig. B2 shows the growth rate $kc_i$ of the unstable barotropic wave in an inviscid fluid and also the function $\nu\alpha k^2$. Waves shorter than the resonant wave, the wavenumber of which is defined by the crossing point of the two curves, damp and longer ones grow with time. In the finite domain used by the numerical integration in this paper, the longest wave in the domain decreases most slowly. It is twice as long as the most unstable wave in an inviscid fluid and, in exp. 1 and 3, it is the nearest wave to the resonant wave. Thus, the longest wave dominates in those experiments.

## References


Abbs, D.J., 1986: Sea-breeze interactions along a concave coastline in southern Australia: Observations and numerical modeling study. *Mon. Wea. Rev.*, **114**, 831–848.

———and R.A. Pielke, 1986: Thermally forced surface flow and convergence patterns over northeast Colorado. *Mon. Wea. Rev. (In* press)

Blumen, W., 1970: Shear layer instability of an inviscid compressible fluid. *J. Fluid Mech.*, **40**, 769–781.

——— and S.C. Dietze, 1981: An analysis of three-dimensional mountain lee waves in a stratified shear flow. *J. Atmos. Sci.*, **38**, 1949–1963.

——— and ———, 1982: An analysis of three-dimensional mountain lee waves in a stratified shear flow: Part II. *J. Atmos. Sci.*, **39**, 2712–2720.

———, P.G. Drazin and D.F. Billings, 1975: Shear layer instability of an inviscid compressible fluid. Part 2. *J. Fluid Mech.*, **71**, 305–316.

——— and C.D. McGregor, 1976: Wave drag by three-dimensional mountain lee-waves in nonplanar shear flow. *Tellus*, **28**, 287–298.

Case, K.M., 1960: Stability of inviscid plane Couette flow. *Phys. Fluids*, **3**, 143–148.

Drazin, P.G. and A. Davey, 1977: Shear layer instability of an inviscid compressible fluid. Part 3. *J. Fluid Mech.*, **82**, 255–260.

Harada, A., 1981: An analysis of the nocturnal cyclonic vortex in the planetary boundary layer of the Kanto plains. *J. Meteor. Soc. Japan*, **59**, 602–610.

Kimura, F., 1986: Formation mechanism of the nocturnal mesoscale vortex in Kanto Plain. Submitted to *J. Meteor. Soc.* Japan.

Satomura, T., 1981a: An investigation of shear instability in a shallow water. *J. Meteor. Soc. Japan*, **59**, 148–167.

———, 1981b: Supplementary note on shear instability in a shallow water. *J. Meteor. Soc. Japan*, **59**, 168–171.

———, 1982: An investigation of shear instability in a shallow water. Part II. *J. Meteor. Soc. Japan*, **60**, 227–244.

Pedlosky, J., 1981: Resonant topographic waves in barotropic and baroclinic flows. *J. Atmos. Sci.*, **38**, 2626–2641.

Szoeke, R.A. de, 1983: Baroclinic instability over wavy topography. *J. Fluid Mech.*, **130**, 279–298.

Wakata, Y. and M. Uryu, 1984: Non-linear behaviors of forced baroclinic wave in a continuous zonal flow. *J. Meteor. Soc. Japan*, **62**, 809–832.

Wendell, L.L., 1972: Mesoscale wind fields and transport estimates determined from a networks of wind towers. *Mon. Wea. Rev.*, **100**, 565–578.

Yoden, S. and H. Mukougawa, 1983: Instability of a baroclinic zonal flow in the presence of surface topography, *J. Meteor. Soc. Japan*, **61**, 789–804.

# 粘性シアー流中の地形性擾乱

里 村 雄 彦
気象研究所応用気象研究部

初期値問題を解くことにより，地形上の粘性シアー流中の擾乱の性質を線形浅水系を用いて解析的および数値的に調べた。解析的な取り扱いにおいては Fourier 変換と Laplace 変換を行って形式解を求め，数値的な取り扱いにおいては平均流を $U=\tanh(y)$, Froude 数を 0.1 として時間積分を行った。その結果以下のことが示される。

非粘性で地形がない場合に不安定であったシアー流は，地形の存在下で粘性を大きくしてゆくと，その安定性が不安定，地形強制と順圧波の共鳴，安定と推移する。安定な領域でも粘性が共鳴を起こす値に近ければ，擾乱は不安定波とほぼ同じ構造を持ち，Reynolds 応力を通じてシアー流からエネルギーを得る。また，地形がシアー流を横切って移動する場合には，不安定波とほぼ同じ構造を持つ渦がシアー帯に残る。この渦もエネルギーをシアー流から得ているために粘性に抗して長時間残っていると解釈される。

粘性が大きい場合，地形強制力をそのまま反映した擾乱が現れる。構造は重力波的であり，そのエネルギーは地形から得ている。

大気中で観測される中規模渦との比較も行う。